Theoretical and Experimental Determination of the Thickness of a Metal Film Grown by Magnetron Sputtering at High Discharge Power

Andrey Tumarkin *, Artem Karamov, Alexey Serdobintsev, Valentin Sakharov, Larisa Volkovoinova, Eugeny Sapego, Alexey Bogdan

Posted Date: 13 December 2024

doi: 10.20944/preprints202412.1095.v1

Keywords: metal film growth; magnetron sputtering; modeling; high discharge power

Article

Theoretical and Experimental Determination of the Thickness of a Metal Film Grown by Magnetron Sputtering at High Discharge Power

Andrey Tumarkin [1,*], Artem Karamov [1], Alexey Serdobintsev [2], Valentin Sakharov [3], Larisa Volkovoinova [2], Eugeny Sapego [1] and Alexey Bogdan [1]

[1] Department of Physical Electronics and Technology, Saint Petersburg Electrotechnical University "LETI", 197022 Saint Petersburg, Russia
[2] Department of Materials Science, Technology and Quality Management, Saratov State University, 410012 Saratov, Russia
[3] Saratov Branch of Kotelnikov Institute of Radioengineering and Electronics RAS, 410019 Saratov, Russia
* Correspondence: avtumarkin@yandex.ru

Abstract: A theoretical model is proposed that allows us to describe the processes of formation of the sputtered atom flow, transport of this flow in the target-substrate space and deposition of the substance onto the substrate during magnetron sputtering. The main difference between the presented model and the existing ones is the combined consideration of the spatial distribution of sputtered atoms and the temperature gradient in the working chamber during magnetron sputtering at high power. To verify the model, real technological parameters of deposition of metal films by magnetron sputtering were used, optimized to achieve a high film growth rate. The agreement between the calculated film thicknesses obtained as a result of modeling and the experimental data was no worse than 5% at discharge powers in the range of 100–700 W. Comparison of the experimental data with the simulation results showed that the model adequately describes the sputtering processes at high discharge powers and low pressures, in contrast to approaches that do not take into account the temperature gradient in the working space.

Keywords: metal film growth; magnetron sputtering; modeling; high discharge power

1. Introduction

Magnetron sputtering is one of the common methods for producing thin-film coatings for the needs of modern electronics. This method is used to form contact layers on the surface of semiconductor circuits, resistive films of hybrid microcircuits, magnetic films, low-resistance contacts, to create new multicomponent thin-film materials, etc. [1–5]. Unlike other methods of film deposition, the magnetron sputtering method allows for fine regulation of the thickness of the metal layer, and hence its resistance, which is very important when creating structures with a certain conductivity. The adhesion of metal layers to the substrate in films obtained by magnetron sputtering is significantly higher than that of the same films obtained by thermal vacuum deposition, at comparable coating growth rates. This is due to the higher energy of condensing particles during magnetron sputtering and additional activation of the substrate surface by the action of plasma.

The properties of thin films (crystallite sizes, defect density, stoichiometry of the film composition and presence of secondary phase inclusions) depend to a significant extent on the conditions under which the coating grows. The characteristics of the gas discharge [6–8], the component composition of the sputtered target [9], the pressure [10] and composition of the working gas [11], the distance between the cathode and the substrate [12] are the main factors that determine

 doi:10.20944/preprints202412.1095.v1

the process of transfer of sputtered atoms in the target-substrate drift space, and, consequently, the final properties of the resulting coating.

The physics of gas discharge and sputtering of various targets has been studied and described in the literature quite well [13–17] and, as a rule, in the case of using standard technological installations for ion-plasma deposition of thin films, does not require separate consideration. The same cannot be said about the processes of transport of sputtered particles through a gaseous medium and condensation on a substrate. These processes are individual [18,19] when sputtering various materials and they will determine the properties of the deposited coating, therefore their study allows us to propose new technological approaches [20,21].

Modeling the processes of transfer of sputtered atoms through a gas medium in the drift space "target-substrate" allows us to estimate the energy characteristics and quantitative ratios of the components arriving at the substrate depending on the process parameters: gas discharge energy, pressure and composition of the working gas, geometric dimensions of the sputtering system. Thus, by modeling the processes of transport of sputtered atoms, it is possible to determine the ranges of process parameters within which it is possible to obtain films with specified characteristics.

All processes occurring during magnetron sputtering can be divided into three main stages: formation of a flow of sputtered atoms, transfer of the substance from the target to the substrate, and deposition on the substrate.

As a result of penetration of the bombarding ion into the target material, a cascade of binary elastic collisions of displaced atoms occurs, in which an exchange of energy and momentum occurs between the atoms. The final result of the collision cascade can be the transfer of sufficient energy and the necessary momentum to the surface atom to overcome the forces of its bond with the surface [22–24].

After leaving the target, the sputtered particles experience collisions with particles of the working gas, losing their energy and changing the direction of movement; some of them may return to the target or diffuse to the walls of the working chamber [25,26]. Modeling the process of transport of sputtered atoms through a gaseous medium from the target to the substrate allows us to determine the intensity of the flow of sputtered particles reaching the substrate, their distribution by energy and the angle of incidence on the substrate.

Atoms of the working substance, moving from the target to the substrate, undergo scattering associated with collisions with atoms of the working gas and the chamber walls, as well as with each other. Depending on the pressure in the chamber, two mechanisms of substance transfer are distinguished: ballistic and diffusion [27,28]. The ballistic mechanism of particle transfer is observed at low pressures of the working gas, when the target-substrate distance is less than or comparable with the mean free path of the sputtered atoms. In this mode, collisions of sputtered atoms with the working gas and with each other can be neglected [29–31]. An increase in the pressure in the chamber leads to an increase in the number of collisions of sputtered atoms with particles of the working gas. As a result, the atoms lose their initial energy and reach the substrate due to diffusion through the gas medium. This mechanism of substance transfer is called diffusion [32–34]. When assessing the number of particles reaching the substrate, it is necessary to take into account both the diffusion and ballistic components.

Estimation of the number of atoms reaching the substrate is a key point for determining the thickness of the formed film and its uniformity [26–28]. Often, when modeling the magnitude of the flow of sputtered particles reaching the substrate, assumptions are used that simplify the calculation, but lead to a decrease in accuracy [28–30]. Among such assumptions, firstly, the position that the spatial distribution of the sputtered substance near the target obeys the cosine law [27], which is true for high energies of sputtering ions [31]. However, at energies of bombarding particles below 1 keV, the distribution of sputtered atoms can deviate significantly from the cosine law, which greatly affects the final number of atoms reaching the substrate [35]. The second assumption considers that the gas temperature is constant throughout the entire space of the working chamber [32–34]. This approach provides good calculation accuracy at low gas discharge powers; however, with increasing power, a divergence of the experimental data and the results of modeling the thickness of the deposited film

 doi:10.20944/preprints202412.1095.v1

is observed. This is due to the fact that at high discharge powers, bombardment of the target with high-energy ions leads to its heating, as well as to an increase in the energy of the sputtered atoms. Both of these factors have a significant effect on the temperature of the gas environment: the target temperature directly, and the energy of the sputtered atoms through collisions with gas particles depending on the pressure. In addition, the substrate can also participate in the heating of the gas if it itself is heated by the condensing particles. This factor must be taken into account if the sputtered particles reach the substrate in a collisionless mode.

In works [33,34], a model for calculating the film thickness is proposed based on an estimate of the number of sputtered particles reaching the substrate. The model takes into account the spatial distribution of sputtered atoms, which differs from the cosine law that allows the film thickness to be calculated with good accuracy in the pressure range from 1 to 10 Pa and at discharge powers of up to 300 W. The gas temperature in these works was assumed to be constant throughout the entire space of the working chamber. In works [36–38] an approach to calculating the gas temperature in the target-substrate space depending on the discharge power and pressure is considered. The authors of works [39–41] calculated the thickness of the deposited film in the pressure range of 1–10 Pa and at powers of up to 250 W taking into account the temperature gradient of the gas in the working volume. Note that these works do not consider the dependence of the spatial distribution of sputtered atoms on the process parameters. In addition, it is assumed that the gas is heated primarily due to energy transfer during collisions of sputtered and gas particles.

Thus, today, a model describing the processes of sputtered particle transport to the substrate in a wide range of discharge powers and working gas pressures, and taking into account the spatial distribution of sputtered atoms, different from the cosine law, the dependence of the gas temperature on the target-substrate distance and the effect of the target and substrate temperatures on it, has not been proposed.

In this regard, we present a model capable of giving an accurate result when calculating the thickness of a metal film deposited in wide ranges of discharge powers. To verify the model, real technological parameters of deposition of metal films by magnetron sputtering were selected. These parameters were optimized to achieve a high film growth rate without deterioration of the coating uniformity. According to our data, this is the first successful attempt to model the thickness of films deposited at high discharge powers and low working gas pressures with an accuracy of no worse than 5% in comparison with the experimental data.

2. Experiment

Chromium (Cr) films were deposited by direct current magnetron sputtering of a 50 mm diameter metal target (99.999% purity, produced by Hyrmet, Russia) using a Robvac VSM300 setup (Russia) onto 30×25×1 mm non-heated glass substrates. The sputtering process was carried out in pure argon (Ar) (99.999% purity, produced by Linde Gas Rus) at a pressure of 0.26 Pa, in the power stabilization mode, the discharge power was 100, 300, 500 and 700 W. The deposition time was 600 s, the target-substrate distance was 90 mm. The edge of the substrate, corresponding to zero along the x-axis, was aligned with the center of the substrate holder, which corresponds to the maximum flux density of the deposited atoms. The thickness of the obtained films was measured using a Dektak 150 profilometer (Veeco Inc., USA) by recording the height profiles. On each sample, the thickness of the chromium film was measured at four points with a step of 1 cm, starting from the projection of the magnetron symmetry axis on the substrate and ending at a distance of 3 cm from it.

3. Description of the Model

The paper considers the geometry of a real magnetron sputtering system with a planar configuration. The water-cooled target has a disk shape and is located parallel under the substrate. Figure 1 shows the geometry of the sputtering system under consideration and the target sputtering zone, the parameters used in the calculation are indicated, and the particle motion trajectories are shown separately for the ballistic and diffusion modes of matter transfer.

 doi:10.20944/preprints202412.1095.v1

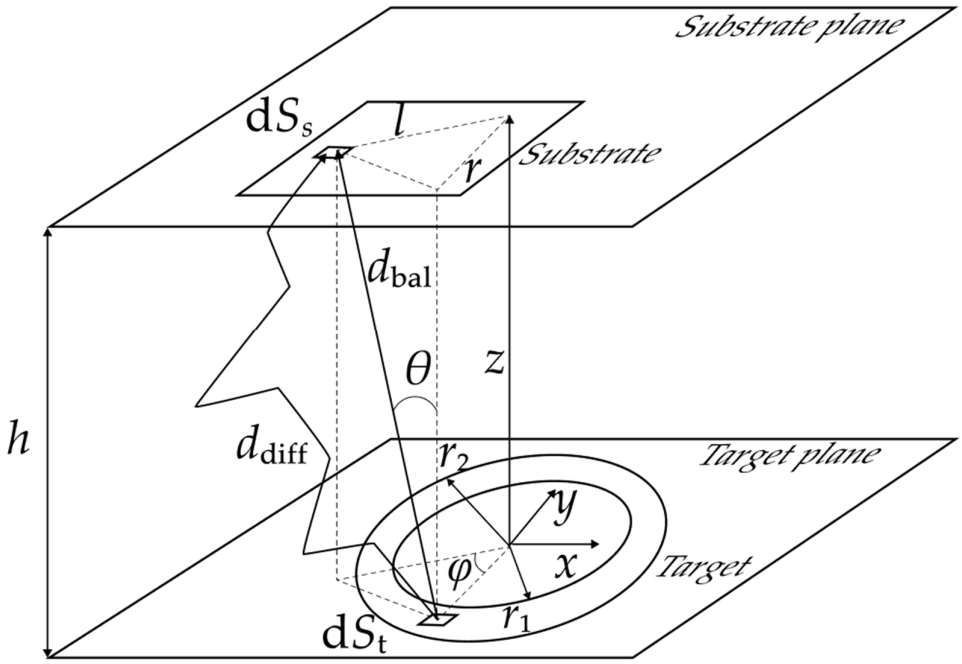

Figure 1. Geometry of the sputtering system used in modeling and in experiment.

In the Figure: h is the shortest target-substrate distance, θ is the angle between the direction of propagation of the atoms and the normal to the target surface, r_1 and r_2 is the external and internal radius of the target erosion zone, d_{diff} is the distance from the source element to the place of deposition of the material during the diffusion transfer of the substance, d_{bal} is the distance from the source element to the place of deposition of the material during ballistic transfer of the substance, φ is the angle between the l and r, where r is the radius-vector from the center of the target to the sputtered area, l is the projection of the radius-vector from the center of the target to the atomic deposition area. dS_t and dS_s are the elementary areas of the target and substrate.

3.1. Target Sputtering

The total number of atoms sputtered from the target was calculated using the formula [42]:

$$j(x) = \frac{I Y}{e\pi (r_1 + r_2)(1+\gamma_{see})} \cdot \frac{f(x)}{\int_0^\infty f(x)\,dx}, \quad (1)$$

where I is the discharge current, Y is the sputtering yield taken from [23], γ_{see} is the secondary electron emission coefficient taken from [24], $f(x)$ is the distribution function that is double semi-Gaussian by coordinate x:

$$f(x) = \begin{cases} \frac{1}{\sqrt{2\pi}\,\Delta} \exp\left[-\frac{(x-\bar{R})^2}{2\Delta_1^2}\right] \text{for } x \le \bar{R} \\ \frac{1}{\sqrt{2\pi}\,\Delta} \exp\left[-\frac{(x-\bar{R})^2}{2\Delta_2^2}\right] \text{for } x > \bar{R} \end{cases}; \quad (2)$$

$$\Delta_1 = \frac{\bar{R} - r_1}{3}, \quad \Delta_2 = \frac{r_2 - \bar{R}}{3}, \quad \Delta = \frac{r_2 - r_1}{6}.$$

 doi:10.20944/preprints202412.1095.v1

where $\bar{R}$ is the middle radius of erosion area; Δ_1, Δ_2, Δ are the standard deviations in the distribution of the flow of sputtered particles.

3.2. Transfer of Working Substance

The total flow of sputtered atoms reaching the substrate is the sum of the diffusion and ballistic components, the ratio of which depends on the working gas pressure and the discharge characteristics:

$$f_{\Sigma} = f_{\text{bal}} + f_{\text{diff}}, \tag{3}$$

where f_{Σ} is the total flux of atoms, f_{bal} is the ballistic flux of atoms, f_{diff} is the diffusion flux of atoms.

In this work, an approach to calculate the total flux of matter taking into account the distribution of sputtered atoms in space, different from the cosine law, presented in detail in [33], was used. The ballistic flow is described by the formula:

$$f_{\text{bal}} = \int_{r_1}^{r_2} \int_{0}^{2\pi} \frac{j(x)\, h^2 (1+\beta (h/d_{\text{bal}})^2)}{d_{\text{bal}}^{\,4}} \exp(-C\, d_{\text{bal}})\, r\, \mathrm{d}r\, \mathrm{d}\varphi, \tag{4}$$

where β is the empirical constant, describing the deviation of the distribution of sputtered atoms from cosine law [35]; d_{bal} is the distance that a sputtered atom travels before deposition on a substrate with a ballistic transfer mechanism $d_{\text{bal}} = \sqrt{(h^2 + r^2 + l^2 - 2rl\cos\varphi)}$; $C = \lambda_s^{-1}$, where λ_s is free path length.

In turn, the ballistic flow is described by the formula:

$$f_{\text{diff}} = \frac{h C\, j_{\Sigma}}{4\pi} \int_{r_1}^{r_2} \int_{0}^{2\pi} \int_{0}^{\infty} \frac{r\ (1+\beta (h/d_{\text{diff}})^2)}{d_{\text{diff}}^{\,3}} \exp(-C\, d_{\text{diff}})\, \mathrm{d}(d_{\text{diff}})\, \mathrm{d}r\, \mathrm{d}\varphi, \tag{5}$$

where d_{diff} is the distance that a sputtered atom travels before deposition on a substrate with a diffusion transfer mechanism, j_{Σ} is the total flux of atoms sputtered from the target, independent of coordinate.

The key difference between formulas 4 and 5 is the geometry of the process of transferring sputtered atoms from the target to the substrate. In ballistic transfer, the spatial distribution of sputtered atoms has a significant effect on the number of particles that reach the substrate, and this distribution must be taken into account when calculating the coating thickness. In diffusion transfer of matter, the trajectory of the atom is chaotic and can tend to infinity. Therefore, to estimate the thickness of the film deposited on the substrate, it is sufficient to determine the total number of sputtered atoms that have reached the substrate.

The length of the free path, taking into account the non-uniformity of the gas temperature in the working volume, is estimated using the formula [27]:

$$\lambda_s(z) = \frac{k\, T(z)}{P\, \sigma}, \tag{6}$$

where k is the Boltzmann constant (J/K), $T(z)$ is the temperature of the working gas (K), P is the working gas pressure (Pa), σ is the collision cross section (m²).

In real magnetron installations for film deposition, there are several process zones, which affect the temperature of the working gas in the vacuum chamber. These include: 1) the target, heated by bombarding ions and cooled from the back; 2) the substrate holder, heated by the energy of the sputtered atoms arriving at the substrate, and/or forced to heat to improve the adhesion of the deposited film and its structure; 3) the working volume itself, the gas temperature in which depends on the frequency of collisions of sputtered atoms with particles of the gas medium. All these factors lead to the emergence of a temperature gradient in the working chamber, to take it into account in the model, the formula is used [41]:

 doi:10.20944/preprints202412.1095.v1

$$T(z) = -\langle E_A \rangle j_\Sigma \frac{p_0 d_0}{\kappa P} \exp\left(-\frac{P z}{p_0 d_0}\right) + c_1 z + c_2, \quad (7)$$

where $\langle E_A \rangle$ is the average kinetic energy of sputtered atoms, $p_0 d_0$ is the characteristic pressure-distance product, κ is the thermal conductivity of the filling argon gas, z is the coordinate along the target-substrate direction, c_1 and c_2 are the constants:

$$c_1 = \frac{1}{h}\left(T_S + \langle E_A \rangle j_\Sigma \frac{p_0 d_0}{\kappa P} \exp\left(-\frac{P h}{p_0 d_0}\right) - c_2\right),$$

$$c_2 = T_T + \langle E_A \rangle j_\Sigma \frac{p_0 d_0}{\kappa P},$$

where T_S is the substrate temperature, T_T is the target temperature.

3.3. Deposition of the Working Substance on the Substrate

The mass of the substance m that reaches the substrate is determined by the total flux of sputtered atoms according to the formula [43]:

$$m = \frac{f_\Sigma M_T}{N_a}, \quad (8)$$

where M_T is the molar mass of the target substance, N_a is the Avogadro constant.

Then the thickness of the film, depending on the coordinate, is determined by the formula:

$$t(r) = \frac{m h^2}{\rho \pi} \frac{h^2 + r^2 + \bar{R}^2}{\left(h^2 + r^2 + \bar{R}^2 + 2\bar{R}r^2\right)^{3/2}\left(h^2 + r^2 + \bar{R}^2 - 2\bar{R}r^2\right)^{3/2}}, \quad (9)$$

where ρ is the density of the target material.

4. Results and Discussion

The thickness of the resulting film and its uniformity are key parameters for conductive coatings and are determined by the number of sputtered particles that reach the substrate. This number, in turn, depends on the discharge power, the geometry of the magnetron sputtering system, and the characteristics of the target material and the working gas. The mass of the atoms of the working gas and target material, as well as the binding energy of the atoms in the target, directly affect the sputtering yield [22]. The discharge power and the geometry of the sputtering system determine the total number of sputtered atoms and its dependence on the coordinate on the target. Figure 2 shows the number of particles sputtered per unit time at different points of the target $j(x)$, which is described by the double Gaussian distribution (2) [42]. The approach to estimating the number of sputtered atoms using formulas (1) and (2) allows one to take into account with high accuracy the geometry of the target erosion zone and the discharge characteristics (power and current density at different points of the target). As expected, an increase in the discharge power leads to a significant increase in the number of sputtered atoms [44] and, consequently, the growth rate of the deposited film. Table 1 presents the experimental characteristics of the discharge, the voltage-dependent energy of the bombarding ions of the working gas (argon) and the calculated values of the number of sputtered particles for different discharge powers obtained using the experimental data.

 doi:10.20944/preprints202412.1095.v1

Table 1. Experimental characteristics of the discharge.

Discharge power, W	Discharge current, mA	Discharge voltage, V	Ion energy, eV	Number of particles, at/s
100	300	313	229	$4.1 \cdot 10^{22}$
300	830	354	259	$1.22 \cdot 10^{23}$
500	1320	375	275	$1.85 \cdot 10^{23}$
700	1740	396	290	$2.35 \cdot 10^{23}$

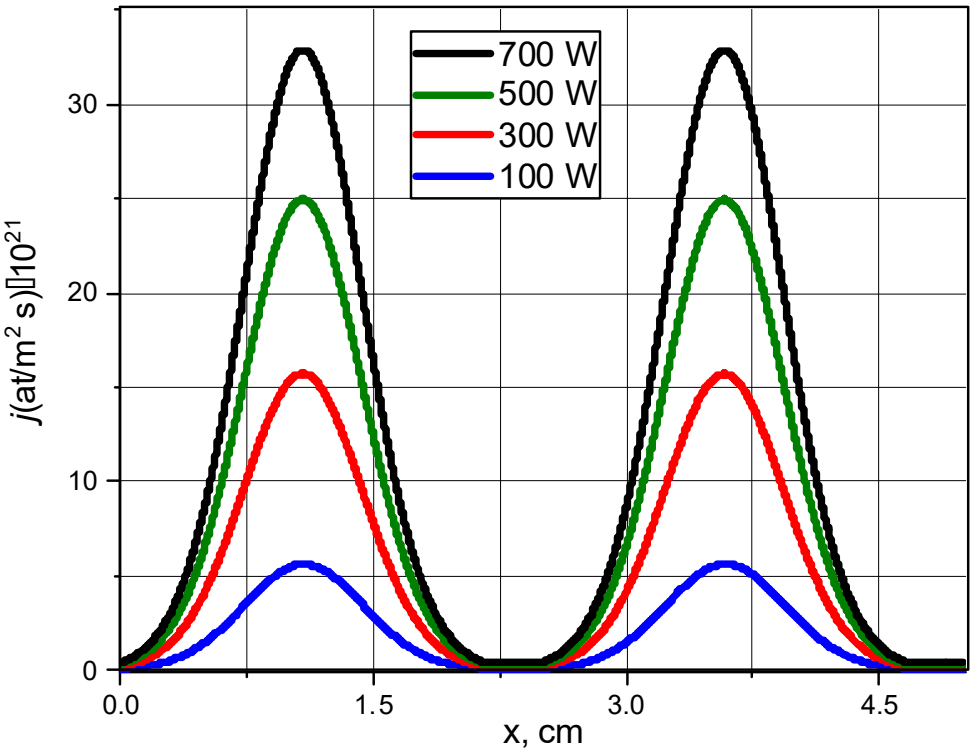

Figure 2. Distribution of the number of sputtered atoms over the target surface at different discharge powers

The main factor determining the number of collisions of sputtered atoms with working gas particles, and hence the coating deposition rate, is the substance transfer mechanism. Figure 3 shows the dependence of the diffusion flux share in the total sputtered atom flux on the working gas pressure for different discharge powers in the considered sputtering system geometry, calculated using formulas (3) - (5). At argon pressures below 1 Pa, the main mechanism of substance transfer from the target to the substrate is ballistic transfer. It can also be noted that with an increase in the discharge power, the diffusion flux share decreases due to an increase in the average energy of sputtered atoms and, consequently, a decrease in the interaction cross-section with an increase in the discharge voltage (see the inset in Figure 3) [33]. The average free path length of sputtered particles at the working gas pressure of 0.26 Pa used in the experiment, calculated using formula (6), ranged from 26 to 43 cm depending on the discharge power, which is significantly greater than the target-substrate distance. At the argon pressure of 0.25 Pa used in our experiment, the proportion of the diffusion flow is about 10%, which makes it necessary to take into account the spatial distribution of sputtered atoms $j(x)$ in calculating the total flow.

 doi:10.20944/preprints202412.1095.v1

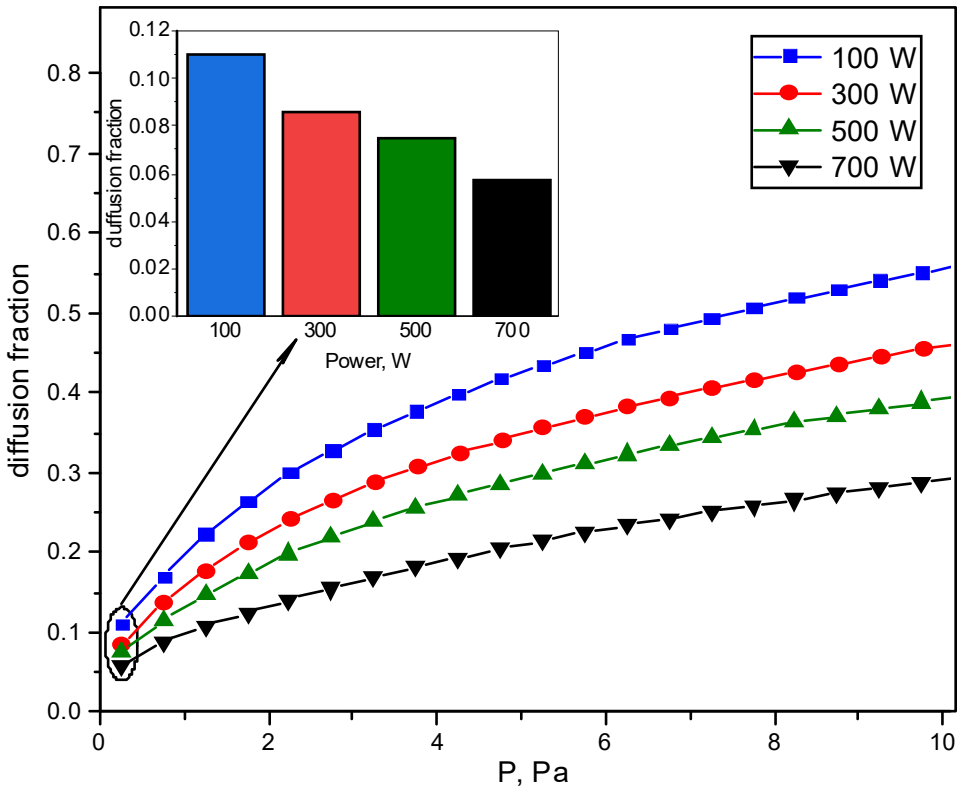

Figure 3. The fraction of the diffusion flow for Cr target sputtering depending on discharge power and pressure; top left is a histogram illustration of the diffusion fraction for working gas pressure used in experiment.

The consequence of the predominance of the ballistic mechanism of mass transfer and the large free path length of the particles is the close-to-linear nature of the dependence of the gas temperature on the target-substrate distance. The dependence of the gas temperature on the distance to the target, calculated using formula (7) at different discharge powers, is shown in Figure 4. The calculation data show that the maximum gas temperature occurs in the region near the target, which is due to its heating as a result of bombardment by ions of the working gas. The target temperature increases from 322 K to 448 K with an increase in the discharge power from 300 to 700 W, due to the increase in the number of ions bombarding the target, as well as the growth of their average energy, the gas temperature also increases along with the target temperature. The target temperature, taking into account its cooling from the back side, was estimated using the technique presented in [45], by solving the three-dimensional homogeneous Fourier equation in a Cartesian coordinate system. Due to the ballistic mechanism of substance transfer and the negligible number of particle collisions in the working chamber, the substrate is heated by the energy of the atoms coming to it. In turn, the substrate does not undergo strong heating due to heat removal through the metal substrate holder.

 doi:10.20944/preprints202412.1095.v1

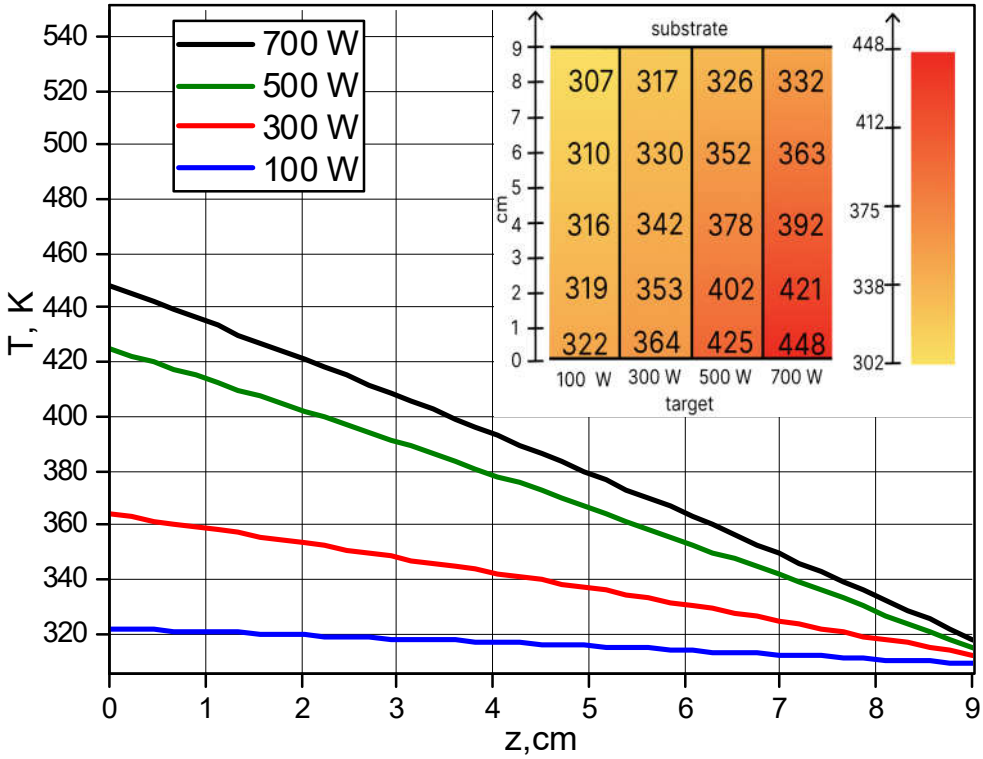

Figure 4. One-dimensional distribution of the gas temperature along the target-substrate distance, top right is a graphical illustration of the temperature distribution.

Since the gas temperature following the target temperature increases with increasing discharge power, one can expect an increase in its influence on the process of transport of sputtered atoms in the working chamber, namely, on the free path length and on the values of ballistic and diffusion flows. To illustrate the influence of the temperature gradient in the target-substrate space on the film deposition process, the expected film thickness at different points of the substrate was calculated using formula (9) taking into account formula (8). Figure 5 shows the experimental and calculated dependences of the chromium film thickness on the substrate coordinate at different discharge powers. In the graph, the red curve indicates the calculated film thickness taking into account the temperature gradient in the working chamber, the blue curve indicates the calculated coating thickness at a constant gas temperature (350 K), estimated by analogy with work [27], the experimental data are marked with squares. The deviation of the chromium film thickness, calculated taking into account the temperature gradient, from the experiment does not exceed 5% in the entire studied range of discharge powers.

It is important to note that at low discharge powers, the calculated film thicknesses with and without taking into account the temperature change in the target-substrate space do not differ much from each other, which is due to slight heating of the gas and a weak dependence of the gas temperature on the target-substrate distance. However, with an increase in the discharge power, the discrepancy between the calculations increases, which can be explained by the increasing influence of the gas temperature on the transport of sputtered atoms. Thus, at a power of 100 W, the discrepancy between the two approaches in the calculation was 6%, while at 700 W the discrepancy was already 12%. Note that in the considered configuration of the sputtering system, a decrease in the film thickness is observed with an increase in the distance from the center of the substrate located above the center of the target. This is due to the static location of the substrate. In further work, it is planned to use substrate rotation to improve the uniformity of the thickness of the deposited film and take into account the rotation in the considered model.

 doi:10.20944/preprints202412.1095.v1

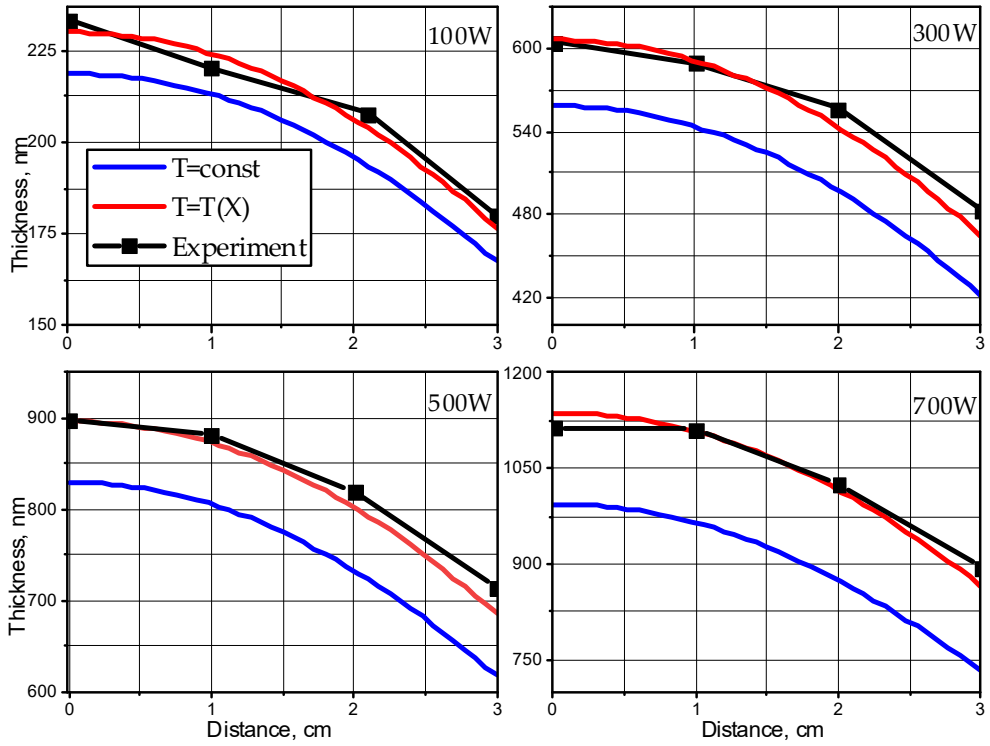

Figure 5. The distribution of film thickness along the substrate for different discharge powers. Black line is the experimental data; red line is the thickness calculated taking into account the temperature gradient; blue line is the thickness calculated at a constant gas temperature.

Figure 6 shows the calculated and experimental data on the chromium film thickness estimate at the substrate point located in the center of the substrate holder (zero on the ordinate axis), depending on the discharge power. The graph clearly shows, firstly, the good agreement between the experiment and the calculation, taking into account the temperature gradient in the target-substrate space, and, secondly, the minor differences in the calculated film thicknesses, for low powers and a significant increase in the discrepancy at high powers for calculations with and without taking into account the change in gas temperature. Thus, taking into account the spatial distribution of sputtered atoms, which differs from the cosine law, as well as taking into account the temperature gradient in the working volume, allows us to adequately estimate the number of sputtered atoms arriving at the substrate and, consequently, calculate the thickness of the deposited film.

 doi:10.20944/preprints202412.1095.v1

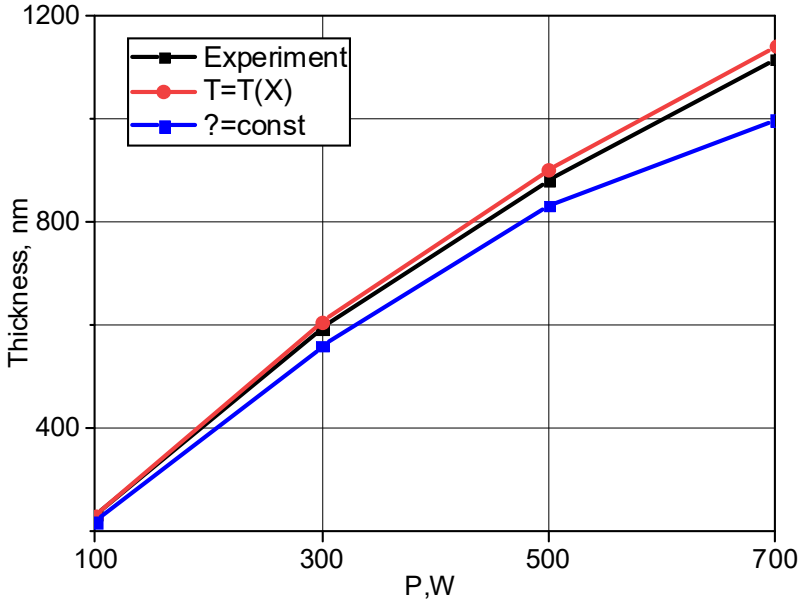

Figure 6. The calculated and experimental data on the chromium film thickness. Black line is the experimental data; red line is the thickness calculated taking into account the temperature gradient; blue line is the thickness calculated at a constant gas temperature.

5. Conclusions

The paper proposes a model that allows quantitative simulation of the processes occurring during magnetron sputtering of a metal target in a wide range of working gas pressures and discharge powers. The processes of sputtered atom flow formation and their transfer to the substrate are considered depending on the technological parameters of the deposition process. This model includes consideration of the spatial distribution of sputtered atoms, different from the cosine law, an estimate of the gas temperature along the target-substrate distance and its effect on the process of sputtered atom transport to the substrate. To verify the model, real technological parameters of metal film deposition by DC magnetron sputtering were used, optimized to achieve a high film growth rate. The model made it possible to obtain a convergence of the calculated film thicknesses with experimental data of no worse than 5% at discharge powers in the range of 100 - 700 W. Comparison of experimental data with simulation results showed that the model adequately describes sputtering processes at high discharge powers and low pressures, in contrast to approaches that do not take into account the temperature gradient in the working space. The results of the work can be useful in developing processes for depositing metal films by magnetron sputtering, which require high coating growth rates. Further research will be aimed at developing the model by taking into account substrate rotation, as well as in relation to sputtering processes of multicomponent targets.

Author Contributions: Conceptualization A.T.; Methodology A.T.; Software A.S. and L.V.; Validation A.T. and A.K.; Investigation A.T., A.K., A.S., V.S., L.V., E.S. and A.B.; Resources A.T. and A.S.; Data Curation A.T.; Writing – Original Draft Preparation A.K.; Writing – Review & Editing A.T. and A.K.; Visualization V.S., A.K., E.S. and A.B.; Supervision A.T.; Project Administration E.S.; Funding Acquisition A.V. All authors have read and agreed to the published version of the manuscript.

Funding: This research was funded by the grant of The Ministry of Education and Science of Russian Federation (project Goszadanie № 075-01438-22-07 FSEE-2022-0015).

Data Availability Statement: The data are contained within the article.

Conflicts of Interest: The authors declare no conflicts of interest.

 doi:10.20944/preprints202412.1095.v1

References

1. Alfonso, E.; Olaya, J.; Cubillos, G. Thin Film Growth Through Sputtering Technique and Its Applications. In *Crystallization - Science and Technology*; Andreeta, M., Ed.; Rijeka Croatia, 2012 pp. 10-21, doi:10.1007/s11664-020-08138-2
2. Rossnagel, S.M. Magnetron Sputtering. *Journal of Vacuum Science & Technology A: Vacuum, Surfaces, and Films* **2020**, *38*, 060805, doi: 10.1116/6.0000594.
3. Gudmundsson, J.T.; Lundin, D. Introduction to magnetron sputtering *Elsevier* **2020**, 1-48, doi: 10.1016/B978-0-12-812454-3.00006-1.
4. Anders, A. Tutorial: Reactive High Power Impulse Magnetron Sputtering (R-HiPIMS) *Journal of Applied Physics* **2017,** *121*, 171101, doi: 10.1063/1.4978350.
5. Baptista, A.; Silva, F.J.G.; Porteiro, J.; Míguez, J.L.; Pinto, G.; Fernandes, L. On the Physical Vapour Deposition (PVD): Evolution of Magnetron Sputtering Processes for Industrial Applications. *Procedia Manufacturing* **2018**, *17*, 746–757, doi: 10.1016/j.promfg.2018.10.125.
6. Jeyachandran, Y.L.; Karunagaran, B.; Narayandass, Sa.K.; Mangalaraj, D.; Jenkins, T.E.; Martin, P.J. Properties of Titanium Thin Films Deposited by Dc Magnetron Sputtering. *Materials Science and Engineering*: *A* **2006**, *431*, 277–284, doi: 10.1016/j.msea.2006.06.020.
7. Muralidhar Singh, M.; Vijaya, G.; Krupashankara, M.S.; Sridhara, B.K.; Shridhar, T.N. Deposition and Characterization of Aluminium Thin Film Coatings Using DC Magnetron Sputtering Process. *Materials Today: Proceedings* **2018**, *5*, 2696–2704, doi: 10.1016/j.matpr.2018.01.050.
8. Wang, S.-F.; Lin, H.-C.; Bor, H.-Y.; Tsai, Y.-L.; Wei, C.-N. Characterization of Chromium Thin Films by Sputter Deposition. *Journal of Alloys and Compounds* **2011**, *509*, 10110–10114, doi: 10.1016/j.jallcom.2011.08.052.
9. Depla, D.; Tomaszewski, H.; Buyle, G.; De Gryse, R. Influence of the Target Composition on the Discharge Voltage during Magnetron Sputtering. Surface and Coatings Technology 2006, 201, 848–854, doi:10.1016/j.surfcoat.2005.12.047.
10. Ahmed, N.; Iqbal, M.A.; Khan, Z.S.; Qayyum, A.A. DC Magnetron-Sputtered Mo Thin Films with High Adhesion, *Conductivity and Reflectance. Journal of Electronic Materials* **2020**, *49*, 4221–4230, doi: 10.1007/s11664-020-08138-2.
11. Paturaud, C.; Farges, G.; Sainte Catherine, M.C.; Machet, J. Influence of Sputtering Gases on the Properties of Magnetron Sputtered Tungsten Films. Surface and Coatings Technology 1996, 86–87, 388–393, doi:10.1016/S0257-8972(96)02954-4.
12. Thaveedeetrakul, A.; Witit-anun, N.; Boonamnuayvitaya, V. The Role of Target-to-Substrate Distance on the DC Magnetron Sputtered Zirconia Thin Films' Bioactivity. Applied Surface Science 2012, 258, 2612–2619, doi:10.1016/j.apsusc.2011.10.104.
13. Gudmundsson, J.T. Physics and technology of magnetron sputtering discharges *Plasma Sources Science and Technology* **2020**, *29*, 113001, doi: 10.1088/1361-6595/abb7bd.
14. Sheridan, T.E.; Goeckner, M.J.; Goree, J. Model of Energetic Electron Transport in Magnetron Discharges. *Journal of Vacuum Science & Technology A: Vacuum, Surfaces, and Films* **1990**, *8*, 30–37, doi: 10.1116/1.577093.
15. Kaziev, A.V. Cathode Sheath Processes in a Non-Sputtering Magnetron Discharge. *Vacuum* **2018**, *158*, 191–194, doi: 10.1016/j.vacuum.2018.09.029.
16. Thornton, J. A. Magnetron sputtering: basic physics and application to cylindrical magnetrons. *Journal of Vacuum Science and Technology* **1978**, *15* (2) 171-177, doi: 10.1116/1.569448.
17. Westwood, W.D.; Maniv, S.; Scanlon, P.J. The Current-Voltage Characteristic of Magnetron Sputtering Systems. *Journal of Applied Physics* **1983**, *54*, 6841–6846, doi: 10.1063/1.332006.
18. Tumarkin, A.V.; Al'myashev, V.I.; Razumov, S.V.; Gaidukov, M.M.; Gagarin, A.G.; Altynnikov, A.G.; Kozyrev, A.B. Structural Properties of Barium Strontium Titanate Films Grown under Different Technological Conditions. *Phys. Solid State* **2015**, *57*, 553–557, doi: 10.1134/S1063783415030348.
19. Lapshin, A.E.; Levitskii, V.S.; Shapovalov, V.I.; Komlev, A.E.; Shutova, E.S.; Myl'nikov, I.L.; Komlev, A.A. Composition and Structure of Copper Oxide Films Synthesized by Reactive Magnetron Sputtering with a Hot Target. *Glass Physics Chemistry* **2016**, *42*, 359–362, doi: 10.1134/S108765961604009X.
20. Tan, X.-Q.; Liu, J.-Y.; Niu, J.-R.; Liu, J.-Y.; Tian, J.-Y. Recent Progress in Magnetron Sputtering Technology Used on Fabrics. *Materials* **2018**, *11*, 1953, doi: 10.3390/ma11101953.
21. Sergievskaya, A.; Chauvin, A.; Konstantinidis, S. Sputtering onto Liquids: A Critical Review. *Beilstein J. Nanotechnology* **2022**, *13*, 10–53, doi: 10.3762/bjnano.13.2
22. Sigmund, P. Theory of Sputtering. I. Sputtering Yield of Amorphous and Polycrystalline Targets. *Physical Review* **1969**, *187*, 768–768, doi: 10.1103/PhysRev.184.383.
23. Behrisch R., Sputtering by particle bombardment. In *Sputtering by Particle Bombardment I*; Behrisch, R., Eds.; Topics in Applied Physics; Publisher: Springer Berlin Heidelberg: Berlin, Heidelberg, 1981; Volume 47, pp. 9–71.

24. Depla, D. On the Effective Sputter Yield during Magnetron Sputter Deposition. *Nuclear Instruments and Methods in Physics Research Section B: Beam Interactions with Materials and Atoms* **2014**, *328*, 65–69, doi: 10.1016/j.nimb.2014.03.001.
25. Gras-Marti, A.; Vallés-Abarca, J.A.; Bensaoula, A. Energy and Momentum Transport by Sputtered and Reflected Streams in a Glow Discharge. *Journal of Vacuum Science & Technology A: Vacuum, Surfaces, and Films* **1987**, *5*, 2217–2221, doi: 10.1116/1.574960.
26. Turner, G.M.; Sikorski, A.; McKenzie, D.R.; Smith, G.B.; Ng, K.; Cockayne, D.J.H. Spatial Variations in the Stoichiometry of Sputtered YBaCuO Thin Films: Theory and Experiment. *Physica C: Superconductivity* **1990**, *170*, 473–480, doi: 10.1016/0921-4534(90)90018-A.
27. Petrov, I.; Ivanov, I.; Orlinov, V.; Sundgren, J.-E. Comparison of Magnetron Sputter Deposition Conditions in Neon, Argon, Krypton, and Xenon Discharges. *Journal of Vacuum Science & Technology A: Vacuum, Surfaces, and Films* **1993**, *11*, 2733–2741, doi: 10.1116/1.578634.
28. Jakas, M.M. Transport Theories of Sputtering. Philosophical Transactions of the Royal Society of London. Series A: Mathematical, Physical and Engineering Sciences **2004**, 362, 139–156, doi: 10.1098/rsta.2003.1305.
29. Ekpe, S.D.; Dew, S.K. Theoretical and Experimental Determination of the Energy Flux during Magnetron Sputter Deposition onto an Unbiased Substrate. *Journal of Vacuum Science & Technology A: Vacuum, Surfaces, and Films* **2003**, *21*, 476–483, doi: 10.1116/1.1554971.
30. Zhang, Y.; Song, Q.; Sun, Z. Research on Thin Film Thickness Uniformity for Deposition of Rectangular Planar Sputtering Target. *Physics Procedia* **2012**, *32*, 903–913, doi: 10.1016/j.phpro.2012.03.655.
31. Revel, A.; Farsy, A.E.; De Poucques, L.; Robert, J.; Minea, T. Transition from Ballistic to Thermalized Transport of Metal-Sputtered Species in a DC Magnetron. *Plasma Sources Science and Technology* **2021**, *30*, 125005, doi: 10.1088/1361-6595/ac352b.
32. Volpyas, V.A.; Kozyrev, A.B. Thermalization of atomic particles in gases. *Journal of Experimental and Theoretical Physics* **2011**, *113*, doi:10.1134/S1063776111060227.
33. Ekpe, S.D.; Bezuidenhout, L.W.; Dew, S.K. Deposition Rate Model of Magnetron Sputtered Particles. *Thin Solid Films* **2005**, *474*, 330–336, doi: 10.1016/j.tsf.2004.09.007.
34. Hong, S.; Kim, E.; Bae, B.-S.; No, K.; Lim, S.-C.; Woo, S.-G.; Koh, Y.-B. A Simulation Model for Thickness Profile of the Film Deposited Using Planar Circular Type Magnetron Sputtering Sources. *Journal of Vacuum Science & Technology A: Vacuum, Surfaces, and Films* **1996**, *14*, 2721–2727, doi: 10.1116/1.580193.
35. Yamamura, Y.; Takiguchi, T.; Ishida, M. Energy and Angular Distributions of Sputtered Atoms at Normal Incidence. *Radiation Effects and Defects in Solids* **1991**, *118*, 237–261, doi:10.1080/10420159108221362.
36. Ekpe, S.D.; Dew, S.K. 3D Numerical Simulation of Gas Heating Effects in a Magnetron Sputter Deposition System. *Journal of Physics D: Applied Physics* **2006**, 39, 1413–1421, doi: 10.1088/0022-3727/39/7/012.
37. Palmero, A.; Rudolph, H.; Habraken, F.H.P.M. Study of the Gas Rarefaction Phenomenon in a Magnetron Sputtering System. *Thin Solid Films* **2006**, *515*, 631–635, doi: 10.1016/j.tsf.2005.12.225.
38. Jimenez, F.; Ekpe, S.D.; Dew, S.K. Inhomogeneous Rarefaction of the Process Gas in a Direct Current Magnetron Sputtering System. *Journal of Vacuum Science & Technology A: Vacuum, Surfaces, and Films* **2006**, *24*, 1530–1534, doi: 10.1116/1.2210005.
39. Sheikin, E.G. The Pressure Dependence of the Deposition Rate in a Magnetron Sputtering System. *Thin Solid Films* **2015**, *574*, 52–59, doi:10.1016/j.tsf.2014.11.043.
40. Palmero, A.; Rudolph, H.; Habraken, F.H.P.M. Gas Heating in Plasma-Assisted Sputter Deposition. *Applied Physics Letters* **2005**, *87*, 071501, doi: 10.1063/1.2010609.
41. Drüsedau, T.P.; Gas heating and throw distance for the sputter deposition of aluminum and tungsten. *Journal of Vacuum Science & Technology A: Vacuum, Surfaces, and Films* **2002**, *20*, 459–466, doi: 10.1116/1.1450586.
42. Golosov, D.; Melnikov, S.; Zavadski, S.; Kolos, V.; Okojie, J. The Increase in Thickness Uniformity of Films Obtained by Magnetron Sputtering with Rotating Substrate. *Plasma Physics and Technology* **2016**, *3*, 100–104, doi: 10.14311/ppt.2016.3.100.
43. Swann, S.; Film thickness distribution in magnetron sputtering. *Vacuum* **1988**, *38(8-10)*, 791–794, doi:10.1016/0042-207X(88)90465-4.
44. Kashtanov, P.V.; Smirnov, B.M.; Hippler, R. Magnetron plasma and nanotechnology *Physics-Uspekhi* **2007**, *50*, 455–488, doi: 10.1070/PU2007v050n05ABEH006138.
45. Kozin, A.A.; Shapovalov, V.I. Modeling of Thermal Processes in Magnetrons with Single Hot Target and "Sandwich-Target." *Surface and Coatings Technology* **2019**, *359*, 451–458, doi: 10.1016/j.surfcoat.2018.12.070.